Shearlet-based measures of entropy and complexity for two-dimensional patterns

Alexey Brazhe*

Department of Biophysics, Faculty of Biology, Moscow State University, Leninskie gory 1/24, 119234 Russia

New spatial entropy and complexity measures for two-dimensional patterns are proposed. The approach is based on the notion of disequilibrium and is built on statistics of directional multiscale coefficients of the fast finite shearlet transform. Shannon entropy and Jensen-Shannon divergence measures are employed. Both local and global spatial complexity and entropy estimates can be obtained, thus allowing for spatial mapping of complexity in inhomogeneous patterns. The algorithm is validated in numerical experiments with a gradually decaying periodic pattern and Ising surfaces near critical state. It is concluded that the proposed algorithm can be instrumental in describing a wide range of two-dimensional imaging data, textures, or surfaces, where an understanding of the level of order or randomness is desired.

I. INTRODUCTION

Spatial patterns with different levels of order and intricacy emerge in the processes of self-organization and morphogenesis, as a result of flow instabilities, as interphase surfaces in systems with criticality. How can one tell if spatial oranization of a pattern is trivial or complex, random, or ordered? Are these properties uniform across the system or can they vary at larger scales? It appears that there is no universal definite answer, as reviewed, e.g., by Crutchfield [1].

Here a practical approach to this problem is proposed in terms of statistics of coefficients of a directional multiscale transform. Additionally, this approach allows for *spatial resolution* of the complexity and randomness properties.

Footprint of a system can be characterized by its location on the complexity-entropy plane [2–4]: A totally ordered periodic structure with a single temporal or spatial scale will have low entropy but also low complexity—simple rules based on a small part are sufficient to reconstruct the full pattern; in the other extreme case of random noise lacking any spatial structure, entropy is maximal, while complexity must again be low—the system is now easily described statistically by a random variable drawn from some distribution. Intermediate cases, on the other hand, can be characterized by high complexity, which makes them more interesting, as they represent systems with nontrivial regularities and correlations in scaling or, in the case of spatially extended signals, in orientation and preferred directions of anisotropic features. Analysis of time series has linked such high-complexity states with systems in a dynamical chaos regime [3]. We note that the theory and method inventory of complexity-entropy relation is much more developed for one-dimensional signals, such as time series, than for higher-dimensional systems. It seems important to be able to distinguish disorder due to randomness and noise from a less trivial one, related to dynamical chaos, fractals, or critical phenomena.

Earlier, Ribeiro *et al.* [5] used a two-dimensional (2D) extension to the permutation entropy of Bandt and Pompe [6] and constructed a method to obtain complexity-entropy pairs for texture images. They used the same intensive entropic nontriviality measure for statistical complexity as introduced by Lamberti *et al.* [4]. This measure is based on the notion of disequilibrium by López-Ruiz *et al.* [2] and is defined in terms of Jensen-Shannon divergence of the observed distribution from an equiprobable one. Recently, Zunino and Ribeiro [7] generalized the original 2D complexity algorithm to obtain multiscale and direction-sensitive estimates of entropy and complexity. The Bandt and Pompe's algorithm relies on ranking signal values within short intervals followed by estimating the distribution of the ordinal permutation patterns. In the 2D domain one clips rectangular patches of the size $D_x \times D_y$, where D_x and D_y are positive integers. The size of the distribution thus grows as $D_x D_y!$ and requires that image size $N_x N_y$ should be at least an order of magnitude larger than that for a reliable estimation [7]. This effectively restricts the application of $(D_x, D_y) > (2,2)$ patches for only very large images.

Spatial structures can also be inhomogeneous, containing isles or gradients of entropy and complexity properties. For example, biological membranes can partition into domains with liquid-ordered (rafts) and liquid-disordered states, influencing also spatial organization of protein complexes [8–10]. One is thus interested in the ability to define spatially resolved measures of entropy and complexity, such that both local and global estimates of these parameters become possible. Accordingly, the goal of this work was to employ an image decomposition system optimally representing anisotropic features at multiple spatial scales to generate structure-related probability distributions sensitive to interscale and directional correlations in the input image. A recently developed shearlets framework [11], which has already found its way into many applications, such as denoising, segmentation, image fusion, and inpainting, seemed the most promising for this goal, as it provides optimally sparse approximation of anisotropic features, is multiscale, uses compactly supported analyzing functions and allows for

---

*brazhe@biophys.msu.ru

efficient implementations. In a nutshell, we substitute the ordinal permutation-derived probabilities of Bandt and Pompe by probabilities based on the power of coefficients of shearlet transform to build the complexity-entropy measures.

The rest of the paper starts with a short description of discrete shearlet transform, followed by plugging it into the entropic nontriviality scheme of Lamberti *et al.* [4]. Next, the utility of the algorithm is demonstrated in controlled numerical experiments, previously employed for illustration of the complexity-entropy analysis in the literature [5,7]. The key innovation of this study is to define *local* spatial entropy in terms of spatially resolved statistics of shearlet coefficients. We then calculate *local* complexity in terms of Jensen-Shannon divergence from the equiprobable distribution. This approach is inherently multiscale and allows for analysis of smaller images than are required by the spatial permutation entropy algorithm.

II. METHODS

A. Inspecting spatial features with shearlet transform

In short, shearlet transform of a digital 2D image $f(x,y)$ is defined in terms of convolution of the image with scaled, sheared, and shifted copies of a specific "mother" shearlet function ψ, thus accounting for different scales and orientations of features contained in the image [11]. To produce modified shearlets, a dilation matrix A_a and a shear matrix S_s are used:

$$A_a = \begin{pmatrix} a & 0 \\ 0 & \sqrt{a} \end{pmatrix}, \quad a \in \mathbb{R}^+, \quad S_s = \begin{pmatrix} 1 & s \\ 0 & 1 \end{pmatrix}, \quad s \in \mathbb{R}. \quad (1)$$

Given shear a, scale s, and translation t, the shearlet function becomes $\psi_{a,s,t} = a^{-3/4}\psi[A_a^{-1}S_s^{-1}(x-t)]$. An example of shearlet at some scale and orientation and its corresponding Fourier image is shown in Fig. 1. Used as a spatial filter, the scaled and shared copies of ψ will emphasize prevalent anisotropic features at different spatial scales and orientations.

In the discrete transform, a fixed number of decomposition scales, shifts, and scale-dependent number of orientations is used with more orientations at higher spatial frequencies. There are several flavors of the discrete shearlet transform. Here we employ a fast finite discrete shearlet transform (FFST) described in detail by Häuser and Steidl [12,13]. Below we provide a minimally sufficient description of the FFST required to build the proposed definition of spatial entropy and complexity. Let us consider the FFST of a square digital image $f \in \mathbb{R}^{N,N}$, which we interpret as a continuous 2D function sampled on a grid $\{m_1/N, m_2/N\}, m \in \mathcal{G}$. Let $j_0 := \lfloor \frac{1}{2}\log_2 N \rfloor$ be the number of considered scales. Under discretization introduced in Ref. [12], the dilation, shear and translation parameters become

$$a_j := 2^{-2j}, \quad j = 0, \dots, j_0 - 1,$$
$$s_{j,k} := k2^{-j}, \quad -2^j \leqslant k \leqslant 2^j,$$
$$t_m := \left(\frac{m_1}{N}, \frac{m_2}{N}\right), \quad m \in \mathcal{G}. \quad (2)$$

This notation leads to the following shearlet definition: $\psi_{j,k,m}(x) := \psi_{a_j, s_{j,k}, t_m}(x) = a^{-3/4}\psi[A_{a_j,\frac{1}{2}}^{-1} S_{s_{j,k}}^{-1}(x - t_m)]$. Note that in Ref. [12] the $a^{-3/4}$ scaling factor is omitted, but we
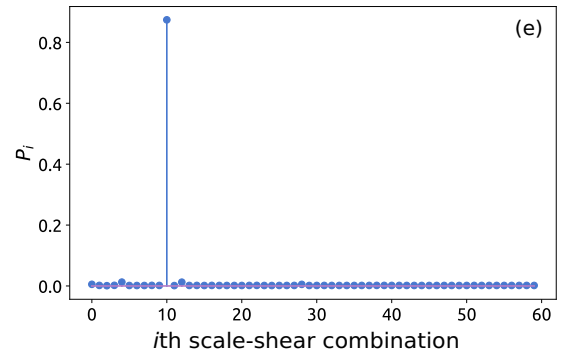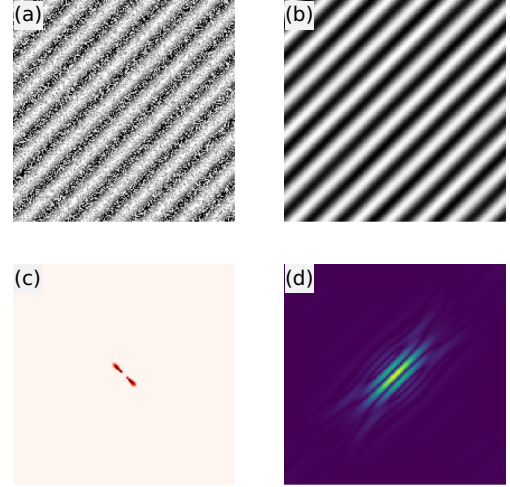

FIG. 1. Example of shearlet transform and shearlet coefficient power distribution. (a) Input image, a striped pattern with added Gaussian noise. (b) Shearlet coefficients $S_{j,k}(x,y)$ for scale and orientation with highest energy of $S_{j,k}$. (c) Corresponding shearlet $|\hat{\psi}_{j,k}|$ in Fourier domain. (d) Corresponding shearlet $\psi_{j,k}$ in image domain. (e) Spectrum of normalized shearlet power at all scale and orientation combinations $\sum_{x,y} S_i^2(x,y)$.

keep it here in order to result in uniform distribution of shearlet coefficient power for spatially uncorrelated random images used as input. Thus, the shearlet transform is defined as a mapping from image f to a set of shearlet coefficients:

$$\mathcal{SH}(f) : f \mapsto \langle f, \psi_{j,k,m} \rangle. \quad (3)$$

Because the translation grid m is scale independent and redundant, the shearlet coefficients can be also represented as a set of images $S_{j,k}(x,y)$ of the same size as f, produced by convolution of $f(x,y)$ with directionally oriented filters of different spatial scales $g_{j,k}$: $S_{j,k} = (f * g_{j,k})(x,y)$. Introducing consecutive indexing i to run though all scales j and shears $s_{j,k}$, we have $\mathcal{SH}(f) := \{S_{j,k}(x,y)\} \equiv \{S_i(x,y)\}$.

The above definition of discrete shearlet transform provides a tight frame: For any image f the following must hold:

$$A\|f\|^2 \leqslant \sum_{j,k,m} |\langle f, \psi_{j,k,m} \rangle|^2 \leqslant B\|f\|^2, \quad (4)$$

where A and B are positive real numbers such that $0 < A \leqslant B < \infty$, and because the frame is tight, $A = B$. This allows us to use normalized power of shearlet coefficients as a descriptor of local feature statistics and interpret it in terms of feature

probability density, which is exploited in the estimate of local structural entropy and complexity in the next section.

B. Shearlet-based entropy and complexity measures

Both entropy and complexity (entropic nontriviality) measures are defined as functionals of some probability distribution $P = \{P_i, i = 1 \dots N\}$. While previous works have employed Bandt and Pompe's permutation entropy [6] for this purpose, we are building our definition based on ideas stemming from the spectral entropy of Powell and Percival [14]. In a similar way as wavelets extend spectral entropy to provide for time-resolved description of one-dimensional signals [15,16], we here propose to use shearlets to provide for a two-dimensional extension of the same measure. Intuitively, the energy of shearlet coefficients $E_i(x,y) = S_i^2(x,y)$ describes how the corresponding scale and orientation is represented at a given location of the image $f(x,y)$. Starting from $E_i(x,y)$ we can define shearlet feature distributions in a global and local settings. In the global case, a single feature distribution is computed for all pixels:

$$P_i^{(g)} = \frac{\sum_{x,y} E_i(x,y)}{\sum_{j,k,x,y} E_{j,k}(x,y)}. \tag{5}$$

The global approach can be used if the image is regarded as a homogeneous pattern, but some images of interest can be inhomogeneous and contain regions of different complexity properties. To provide for a spatially resolved estimate, we use locally averaged (Gauss-blurred) shearlet power coefficient images $E_i^*(x,y) := (K_{\sigma_j} * E_i)(x,y)$ to define a local shearlet feature distribution:

$$P_i^{(l)}(x,y) = \frac{E_i^*(x,y)}{\sum_{j,k} E^*(x,y)}, \tag{6}$$

thus interpreting a spectrum of local feature scales and orientations as a density function. Here $(K_\sigma * \cdot)$ denotes convolution with a Gaussian kernel of standard deviation σ. Scale-dependent $\sigma_j = \sigma_0 2^{j_0-j-1}$ are used to allow for wider neighborhood at larger spatial scales.

Based on the obtained probability distribution $P = \{P_i\}$ we define Shannon entropy $S[P] = -\sum_i P_i \log_2 P_i$, and normalized entropy $H_s[P] = S[P]/S[P_e]$, where $S[P_e] = S_{max} = \log_2 N$ for the equiprobable or uniform distribution P_e, where all shearlet features are equally presented $P_i = 1/N, | i = 1 \dots N$. In a similar way to Ribeiro *et al.* [5] and Zunino and Ribeiro [7], we use a disequilibrium-based statistical measure of complexity $C[P]$ introduced by López-Ruiz *et al.* [2]:

$$C[P] = Q_{JS}[P, P_e] H_S[P], \tag{7}$$

where, following Lamberti *et al.* [4] and Rosso *et al.* [17], we employ normalized Jensen-Shannon divergence $Q_{JS} = J[P, P_e]/J_{max}$ as disequilibrium measure, which describes a distance between an observed (P) and the equiprobable (P_e) distributions:

$$J[P, P_e] = S\left[\frac{P + P_e}{2}\right] - \frac{1}{2}(S[P] + S[P_e]). \tag{8}$$

Clearly, $J[P, Pe] = 0$ if $P = P_e$ and is maximal when only one feature, say, mth, is present, while all others are ab-

sent: $P_i = 1 | i = m$, $P_i = 0 | i \neq m$, $J_{max} = -\frac{1}{2}[\frac{N+1}{N} \log_2 (N+1) - 2\log_2 2N + \log_2 N]$.

The obtained complexity measure quantifies both randomness and degree of spatial correlations in the data, and thus for each entropy value H there exists a range of admissible complexity C values between a lower C^{min} and upper C^{max} bounds [2,3,18]. For a distance measure based on Jensen-Shannon divergence, the lower bound is found by a family of distributions where one of the outcomes P_i has probability $P_i = \frac{1}{N} \dots 1$ and the rest P_j have uniform probabilities $P_j = \frac{1-P_i}{N-1} | j \neq i$. The upper bound is formed by distributions with $n < N$ outcomes having probabilities $P_i = \frac{1}{n}, i = 1, \dots, n$ and the rest having zero probabilities $P_j = 0, j = n+1, \dots, N$.

In recapitulation, the normalized power of shearlet coefficients is interpreted as a probability distribution, which is next compared to an equiprobable and a singular distributions in order to define spatial entropy and complexity measures.

The software and example code needed to compute the shearlet-based spatial entropy and complexity estimates will be available open source at [19].

III. RESULTS OF NUMERICAL EXPERIMENTS

The proposed approach is tested in two computational experiments of the same kind as used in the literature [5,7]: (i) gradually randomized periodic pattern and (ii) simulated Ising surface around critical temperature. In the first experiment we observe nonmonotonic change of complexity with noise level, and in the second the phase transition is clearly reflected in the entropy and complexity values.

A. Gradual randomization of a periodic grid pattern

We start with a periodic pattern of regularly spaced grayscale stripes. The original pattern is gradually corrupted by setting, with some probability, pixel values to a random grayscale level [Fig. 2(a)]. Shearlet-based spatial entropy monotonically rises from zero to one with pixel defacing probability, while the complexity estimate reaches a peak value of around $C = 0.2$ at $p \approx 80\%$ [Fig. 2(b)]. The qualitative picture is in a good agreement with results based on permutation entropy [7], but in the current work the peak in complexity is lower and is reached at a higher noise level. This discrepancy can in part be explained by the difference in algorithms and in part by dependence of the complexity peak position on spatial frequency of the grid (not shown).

The observed dependence of entropy and complexity on deface probability is quite intuitive. The original pattern is ordered, and the shearlet coefficients are dominated by those matching the stripe scale and orientation as exemplified by Figs. 1(a)–1(d). Hence the distribution of coefficient power is far from equiprobable, which leads to zero entropy and maximal Jensen-Shannon divergence. Because complexity is a product of normalized entropy and disequilibrium, it is zero, too. With adding increasing levels of noise the entropy predictably rises, while remains of the ordered structure visible behind the noise make the pattern complex, and complexity peaks almost just before the ordered structure is completely lost $p \approx 0.8$. With $p = 1$ the input image becomes featureless independent and identically distributed Gaussian noise and
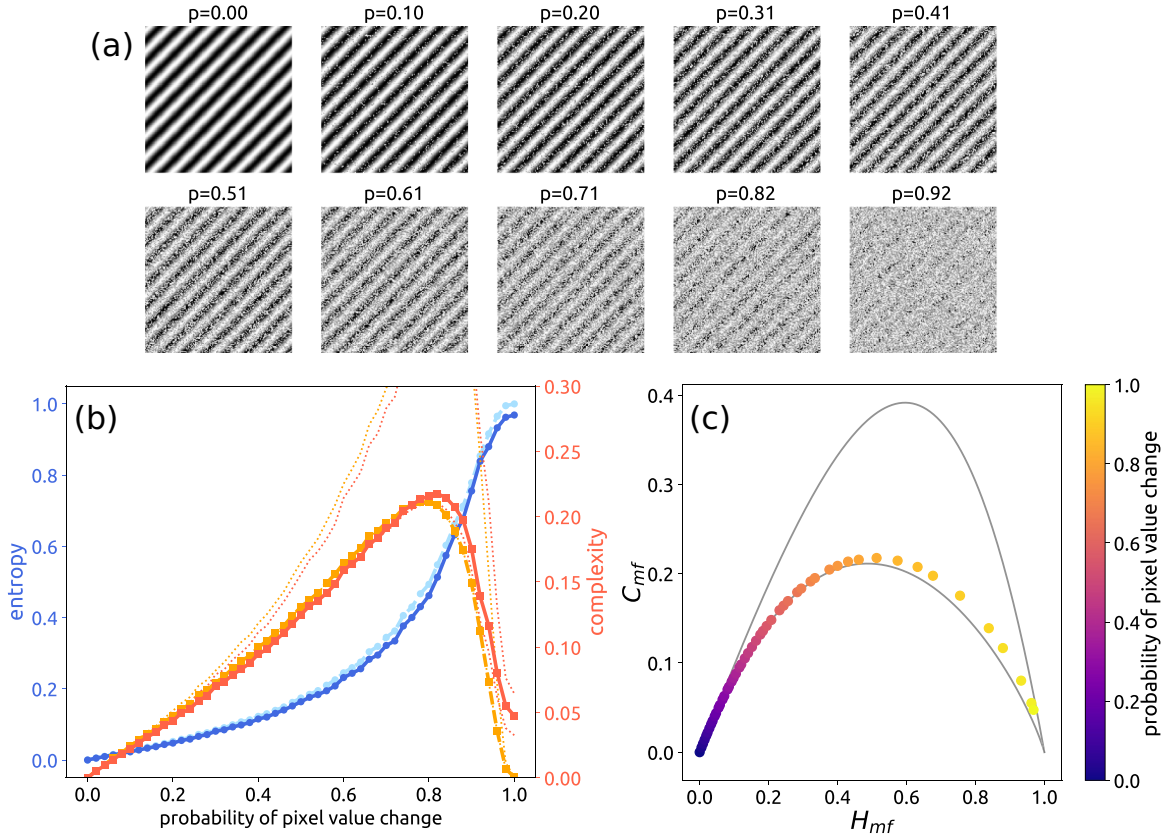
FIG. 2. Evolution of entropy and complexity in gradually randomized periodic patterns. (a) Input images with different probabilities of pixel value change shown on top; image size: 280×280. (b) Entropy (blue) gradually rises with increase in probability of pixel value change, while complexity behavior is nonmonotonic (orange and red). Light-blue and orange lines, global estimate; dark-blue and red lines, "mean field" estimate. Dotted line, admissible complexity C range for given entropy H. (c) Same as in (b) but plotted on the H–C plane for "mean-field" estimates; pixel probability change is color coded. Region enclosed in the thin gray line, the admissible complexity range.

thus shearlet coefficients are nearly uniformly distributed, leading to maximal entropy and zero disequilibrium and hence complexity.

Thus, as a regular ordered state dissolves, the complexity will reach a peak value, while entropy will rise monotonically, which is also in agreement with similar results obtained for equilibration in closed systems [20]. It is also clear that the pixel defacing process in this experiment is equivalent to swapping pairs of pixels at random in the image, which would make the system analogous to that of Aaronson *et al.* [20].

There are two pairs of complexity-entropy curves in Fig. 2(b): The dashed line corresponds to a global definition of shearlet-based probability (5), while the solid line is derived from the local definition (6) by averaging the $H[P(x,y)]$ and $C[P(x,y)]$ values over the image domain and denoted as a "mean-field" estimate in the rest of the text. The two estimates are congruent because of the uniform dominating regular pattern. This agreement between the global and mean-field estimates does not always have to hold: For example, a number of small-scale anisotropic structures with high spatial complexity randomly dispersed in an input image will result in low global complexity due to spatial averaging of inputs from $S_{j,k}^2$ at different orientations but can have a large mean-field complexity. The discrepancy between the global and mean-field estimates becomes more evident in the next section.

Interestingly, despite the transient rise, the complexity levels for decaying regular pattern remain on the lower bound of the admissible complexity level [shaded regions in Figs. 2(b) and 2(c)]. Thus, equilibration of a closed system follows the path of minimal possible complexity. The next section demonstrates that the situation is different for a critical system.

B. Ising surfaces

We next turn to the analysis of rough surfaces induced by two-dimensional lattice spin models described by Brito *et al.* [21,22]. Specifically, it is interesting to test whether the proposed approach will be able to capture spatial complexity and entropy changes associated with phase transition. Here the surfaces are built by summing up the lattice spin values $\sigma_l = \{-1,1\}$ of the spin-1/2 Ising model defined by the Hamiltonian:

$$\mathcal{H} = - \sum_{\langle m,n \rangle} \sigma_m \sigma_n , \qquad (9)$$

where the summation runs over all $\langle m,n \rangle$ pairs of nearest-neighbor nodes. This system undergoes phase transition at $T_c = \frac{2}{\ln(1+\sqrt{2})}$. The model was simulated with a Monte Carlo algorithm on 256×256 lattices. Surface height at a site l at simulation step t is then defined as $W_l = \sum_{k=0}^{t} \sigma_l(t)$. Examples of the obtained surfaces at different reduced temperatures
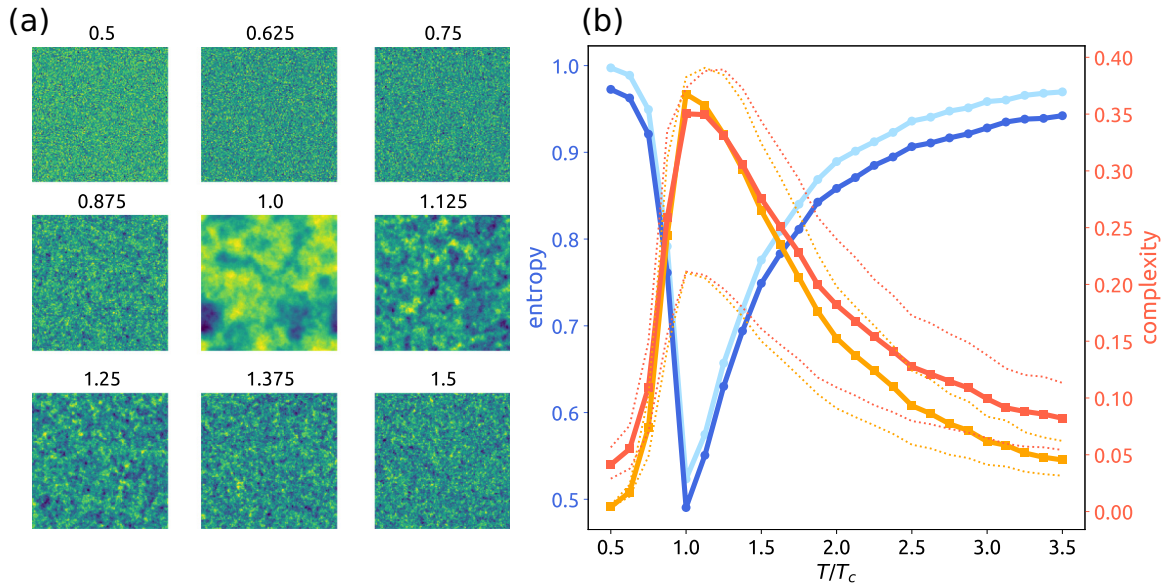
FIG. 3. Ising surfaces and temperature dependence of complexity and entropy properties. (a) Examples of simulated Ising surfaces at different reduced temperature levels $T_r = T/T_c$ shown on top (image size: 256×256, after 3×10^4 iterations; image intensities are renormalized to $0 \dots 1$ interval for better representation). (b) Dependence of entropy (blue) and complexity (orange and red) on reduced temperature. The critical temperature is characterized by a peak in complexity and a dip in entropy. Light-blue and orange lines, global estimate; dark-blue and red lines, "mean field" estimate. Dotted lines, admissible complexity C range for given entropy H. Dotted lines, admissible complexity C range for given entropy H.

$T_r = T/T_c$ after 3×10^4 Monte Carlo steps are shown in Fig. 3(a).

As expected, both spatial entropy and complexity parameters undergo dramatic changes as the reduced temperature sweeps through the critical point $T_r = 1$: the critical temperature is associated with a peak in system complexity and a negative peak in entropy [Fig. 3(b)]. Thus, the temperature of phase transition is characterized by maximal complexity and minimal entropy of the analyzed spatial pattern. Indeed, a critical state leads to emergence of scale-free spatial structure with marked spatial correlations. As in wavelets for time series, one can expect a power-law scaling of the power of shearlet coefficients, which should lead to high complexity and intermediate entropy.

One also observes from Fig. 3(a) that at temperatures slightly larger than T_c the spatial correlations in the structure do not vanish immediately, and the images remain "grainy" for about $T_r \approx 1.25$. Existence of isles with higher spatial correlations leads to asymmetric dependence of both entropy and complexity on temperature: The changes are steeper for temperatures below T_c than for $T > T_c$, so the complexity falls off slower with an increase than with a decrease in temperature. Higher temperatures are also characterized by a larger discrepancy between the global and the "mean-field" estimates of H and C: Here $H_{MF} < H_{global}$ and $C_{MF} > C_{global}$, which can be explained by existence of small isles of higher complexity, which are attenuated by spatial averaging of the shearlet coefficients in the global estimate but not in the "mean-field" one.

Again, the obtained results are qualitatively similar to the analogous experiment in Ref. [5]: The H and C parameters change in the same direction and display the same asymmetry with respect to temperature change. However, the changes in both H and C are more pronounced with the proposed method: Entropy reaches a smaller minimal value of $H_{T_c} \approx 0.5$ and complexity peaks at a higher level $C_{T_c} \approx 0.35$. In addition, we note that near T_c the system nearly reaches the maximum complexity C^{max} allowed for the corresponding entropy value [see also Fig. 4(b)]. This is dramatically different from the previous example with decaying structure, where the complexity remained near C^{min}.

The main novelty of the proposed method as compared to the method suggested by Ribeiro *et al.* [5] is that the shearlet-based approach allows for *spatially resolved estimates* of complexity $C(x, y)$ and entropy $H(x, y)$ as illustrated in Fig. 4(a), where the H and C estimates are mapped for an Ising surface at $T = T_c$. Thus, an input image can be characterized not with a single (H, C) pair but with a complexity-entropy spectrum, representing distribution of all spatial locations of the analyzed pattern on the complexity-entropy plane. Such spectra are shown together with "mean-field" and global estimates for Ising surfaces at several temperatures around the critical one in Fig. 4(b). Here one can see that the relation between the entropy and complexity for points belonging to one image can be markedly different depending on the location on the complexity-entropy plane. In all cases the Ising surface remains well above C^{min}. Moreover, near the T_c, the complexity-entropy spectra concentrate around the curve corresponding to a set of power-law distributions depicted as a gray line in Fig. 4(b). This supports the expectation that shearlet coefficients should have power-law statistics for a spatially scale-free pattern. Above T_c, spatial inhomogeneities acquire characteristic scale which gradually shrinks with temperature—reflected in deviation from the complexity-entropy spectra from the power-law curve.
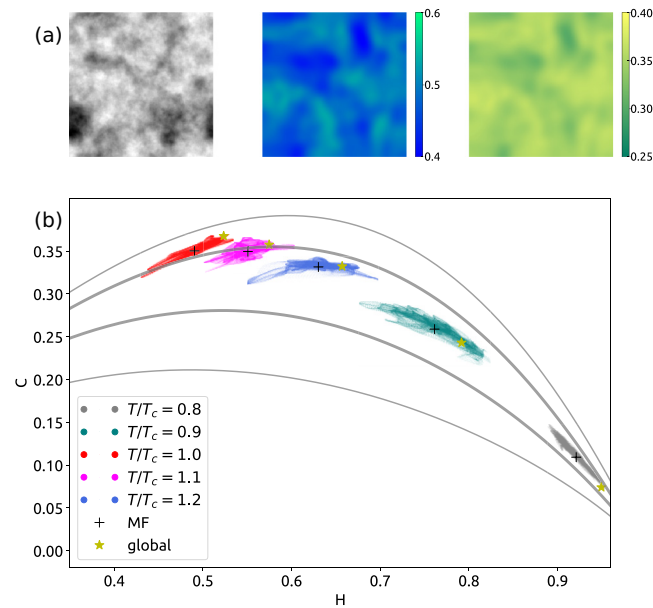
FIG. 4. Spatial mapping of local complexity and entropy and complexity-entropy spectra for Ising surfaces. (a) Ising surface at $T = T_c$ (left), local entropy (middle), and complexity (right). (b) Complexity-entropy spectra taken from local values and shown on the H–C plane for Ising surfaces at different temperatures. Crosses, average, "mean field" values; stars, global estimates. Thin gray line encircles the admissible complexity C range for each H value. Thick gray line, point curve corresponding to power-law distributions.

IV. CONCLUSIONS

An algorithm of estimating empirical spatial entropy and complexity measures for two-dimensional patterns or texture images is proposed. The algorithm builds on recent success in employing a two-dimensional extension to the Bandt and Pompe's permutation entropy augmented with a Jensen-Shannon–based definition of statistical nontriviality (complexity). The core difference of the proposed algorithm is that it replaces the permutation approach by a new probability-inducing decomposition of spatial patterns based on an efficient multiscale directional transform, namely the fast finite shearlet transform. In other words, it generalizes the ideas of wavelet entropy to higher-dimensional data by using an adapted decomposition system. Besides computational efficiency, the proposed algorithm provides for local, spatially resolved estimates

of complexity and entropy of the analyzed pattern, which was not possible with previous algorithms.

Numerical experiments with two classes of spatial patterns support the utility of the proposed method, as the expected changes in both entropy and complexity associated with changes in the controlled parameters are faithfully captured in the estimates provided by the algorithm. These two different systems, although both undergoing a rise and fall in complexity, behave differently in the complexity-entropy plane as compared to whether they are close to the lower or higher bounds of complexity. Attaining a max-entropy equilibrium from an ordered state follows a minimum possible complexity path, which seems to be at odds with Ref. [23], where a tendency towards maximum complexity has been reported. Calbet and López-Ruiz [23] used a Euclidean distance measure of dissimilarity between the observed and equiprobable distributions as originally suggested by López-Ruiz *et al.* [2], which has troublesome characteristics, remedied by the use of the Jensen-Shannon divergence measure [4], which can explain the apparent discrepancy of the results. In contrast, the Ising surface model was characterized by complexity values closer to the upper bound, and near the critical point was in agreement with a scale-free structure governed by a power-law distribution of feature scales and orientations. One can thus discriminate between *intrinsic* complexity, resulting from the system properties and foraying into high-complexity regions towards the upper complexity bound, and *extrinsic* complexity, appearing, e.g., due to remains of ordered state melted by noise, in which case the complexity keeps to near the lower bound.

The paper is accompanied by an open-source python-based software and a usage example in the form of a jupyter notebook, thus prompting other research groups for employment of the proposed algorithm in problems where a global or spatially resolved characterization of textures is required. It is expected that this method will be instrumental in the analysis of cell or tissue morphology in microscopy data, characterization of patterns in the studies of hyperuniformity packing, description of fiber networks, displacement landscapes in oil and water flooding, and other applications.

[1] J. P. Crutchfield, Nat. Phys. **8**, 17 (2012).

[2] R. López-Ruiz, H. Mancini, and X. Calbet, Phys. Lett. A **209**, 321 (1995).

[3] O. A. Rosso, H. A. Larrondo, M. T. Martin, A. Plastino, and M. A. Fuentes, Phys. Rev. Lett. **99**, 154102 (2007).

[4] P. W. Lamberti, M. T. Martin, A. Plastino, and O. A. Rosso, Physica A **334**, 119 (2004).

[5] H. V. Ribeiro, L. Zunino, E. K. Lenzi, P. A. Santoro, and R. S. Mendes, PLoS ONE **7**, e40689 (2012).

[6] C. Bandt and B. Pompe, Phys. Rev. Lett. **88**, 174102 (2002).

[7] L. Zunino and H. V. Ribeiro, Chaos, Solitons Fractals **91**, 679 (2016).

[8] R. M. Henderson, J. M. Edwardson, N. A. Geisse, and D. E. Saslowsky, Physiology **19**, 39 (2004).

[9] D. Owen and K. Gaus, Front. Plant Sci. **4**, 503 (2013).

[10] E. Sezgin, I. Levental, S. Mayor, and C. Eggeling, Nat. Rev. Mol. Cell Biol. **18**, 361 (2017).

[11] G. Kutyniok and D. Labate, *Shearlets: Multiscale Analysis for Multivariate Data* (Birkhauser, Basel, 2012).

[12] S. Häuser and G. Steidl, arXiv:1202.1773 (2012).

[13] S. Häuser and G. Steidl, Int. J. Comput. Math. **90**, 62 (2013).

[14] G. E. Powell and I. C. Percival, J. Phys. A: Math. Gen. **12**, 2053 (1979).

[15] R. Q. Quiroga, O. A. Rosso, E. Başar, and M. Schürmann, Biol. Cybern. **84**, 291 (2001).

[16] O. A. Rosso, S. Blanco, J. Yordanova, V. Kolev, A. Figliola, M. Schürmann, and E. Başar, J. Neurosci. Methods **105**, 65 (2001).

[17] O. A. Rosso, L. Zunino, D. G. Pérez, A. Figliola, H. A. Larrondo, M. Garavaglia, M. T. Martán, and A. Plastino, Phys. Rev. E **76**, 061114 (2007).

[18] M. T. Martin, A. Plastino, and O. A. Rosso, Physica A **369**, 439 (2006).

[19] https://github.com/abrazhe/shearlexity.

[20] S. Aaronson, S. M. Carroll, and L. Ouellette, arXiv:1405.6903.

[21] A. F. Brito, J. A. Redinz, and J. A. Plascak, Phys. Rev. E **75**, 046106 (2007).

[22] A. F. Brito, J. A. Redinz, and J. A. Plascak, Phys. Rev. E **81**, 031130 (2010).

[23] X. Calbet and R. López-Ruiz, Phys. Rev. E **63**, 066116 (2001).